2668 *Chem. Mater.* **2010,** *22,* 2668–2674
DOI:10.1021/cm100173p

CHEMISTRY OF MATERIALS
Article

Synthesis and Crystal Structure of Lanthanide Orthoniobates Studied by Vibrational Spectroscopy

Kisla P. F. Siqueira,[†] Roberto L. Moreira,[‡] and Anderson Dias*[,†]

[†]*Departamento de Química, Universidade Federal de Ouro Preto, Campus Morro do Cruzeiro, ICEB II, Ouro Preto-MG 35400-000, Brazil, and* [‡]*Departamento de Física, Universidade Federal de Minas Gerais, C.P. 702, Belo Horizonte-MG 30123-970, Brazil*

Received January 20, 2010. Revised Manuscript Received February 25, 2010

$RENbO_4$ (RE = La, Ce, Pr, Nd, Sm, Eu, Gd, Tb, Dy, Ho, Er, Tm, Yb, Lu) materials were synthesized by solid-state reactions and then systematically investigated by vibrational spectroscopy. Single-phase materials were obtained at optimized temperature and time conditions, which were probed by X-ray diffraction and Raman scattering. Vibrational spectroscopy was employed to investigate the crystal structure of the lanthanide orthoniobate series by using different excitation lines in the visible region and also infrared techniques. All $RENbO_4$ ceramics exhibited a monoclinic structure, space group $C2/c = C_{2h}^6$ (No. 15), with $Z = 4$. Raman spectroscopy evidenced 18 modes whose symmetries could be discerned by using polarized scattering, in perfect agreement with group theoretical calculations. The wavenumbers of the active-bands presented generally a decreasing tendency for increasing RE ionic radii, as a consequence of the lanthanide-induced lattice expansion. Fourier-transform infrared spectroscopy was employed to study the optical polar phonons of a typical lanthanide orthoniobate material. The results showed 15 active modes, as predicted by the group-theory for these compounds. Kramers−Krönig analysis was used to corroborate the results obtained after fitting and to establish a complete set of $RENbO_4$ active phonons, not yet reported in the literature.

Introduction

ABO_4 ternary oxides are very attractive materials from the chemical point of view because of their ability to combine chemical elements in this basic formula, which lead to an incredibly wide array of structures and phases with totally different functions. Nowadays, a huge number of "old" and "new" compounds are being studied by a wide scientific community in the framework of their crystal chemistry toward emerging applications: ferroelastics,[1] scintillating crystals,[2] chemically robust hosts for nuclear materials and wastes,[3] Raman lasers,[4] cryogenic phonon-scintillation detectors,[5] protonic conductors,[6] and photocatalysts,[7] among other optoelectronic devices. Recently, rare-earth orthoniobates ($RENbO_4$) have attracted much attention because of their mixed protonic, native ionic, and electronic conduction properties.[6] Also, the discovery of new phases and morphologies expanded the field of rare-earth (RE) orthoniobate and orthotantalate chemistry toward multiple energy applications.[8]

In this respect, it is recognized that the behavior of functional materials is directly linked to their structures, which in turn are frequently studied by techniques like X-ray and neutron diffraction, infrared spectroscopy and Raman scattering. Our group uses vibrational spectroscopy to probe structural features, crystal chemistry, and phase transitions in electroceramics.[9−11] In this paper, we report for the first time the synthesis of the complete lanthanide-orthoniobate series (La−Lu, excluding radioactive promethium) in conjunction with a detailed structural investigation through Raman scattering and Fourier-transform infrared spectroscopy. Previous papers have studied the synthesis and properties of some RE orthoniobates, including Lu,[1,12] Yb,[6,13] Er,[1,14] Tb,[6] Ho,[15] Dy,[1,15] Eu,[15] Gd,[6,12] Sm,[1,15] Nd,[1,16] Pr,[15] Ce,[15] and La, the most studied orthoniobate compound.[1,6,15−17]

*Corresponding author. Tel.: 55-31-3559-1716. E-mail: anderson_dias@iceb.ufop.br.

(1) Kim, D. W.; Kwon, D. K.; Yoon, S. H.; Hong, K. S. *J. Am. Ceram. Soc.* **2006**, *89*, 3861.
(2) Annenkov, A. A.; Korzhik, M. V.; Lecoq, P. *Nucl. Instrum. Methods Phys. Res. A* **2002**, *490*, 30.
(3) Weber, W. J.; Ewing, R. C.; Catlow, C. R. A.; de la Rubia, T. D.; Hobbs, L. W.; Kinoshita, C.; Matzke, H.; Motta, A. T.; Nastasi, M.; Salje, E. K. H.; Vance, E. R.; Zinkle, S. J. *J. Mater. Res.* **1998**, *13*, 1434.
(4) Brenier, A.; Jia, G.; Tu, Ch. *J. Phys.: Condens. Matter.* **2004**, *16*, 9103.
(5) Angloher, G.; Bruckmayer, M.; Bucci, C.; Buhler, M.; Cooper, S.; Cozzini, C. *Astropart. Phys.* **2002**, *18*, 43.
(6) Hausgrud, R.; Norby, T. *Nat. Mater.* **2006**, *5*, 193.
(7) Machida, M.; Murakami, S.; Kijima, T.; Matsushima, S.; Arai, M. *J. Phys. Chem. B* **2001**, *105*, 3289.
(8) Nyman, M.; Rodriguez, M. A.; Rohwer, L. E. S.; Martin, J. E.; Waller, M.; Osterloh, F. E. *Chem. Mater.* **2009**, *21*, 4731.
(9) Dias, A.; Subodh, G.; Sebastian, M. T.; Lage, M. M.; Moreira, R. L. *Chem. Mater.* **2008**, *20*, 4347.
(10) Dias, A.; Matinaga, F. M.; Moreira, R. L. *Chem. Mater.* **2007**, *19*, 2335.
(11) Moreira, R. L.; Feteira, A.; Dias, A. *J. Phys.: Condens. Matter.* **2005**, *17*, 2775.
(12) Xiao, X.; Yan, B. *J. Non-Cryst. Solids* **2005**, *351*, 3634.
(13) Jehng, J.; Wachs, I. E. *Chem. Mater.* **1991**, *3*, 100.
(14) Zhang, De-L.; Hua, P. R.; Pun, E. Y. B.; Siu, G. G. *J. Am. Ceram. Soc.* **2007**, *90*, 2893.
(15) Octaviano, E. S.; Ardila, D. R.; Andrade, L. H. C.; Li, M. S.; Andreeta, J. P. *Cryst. Res. Technol.* **2004**, *39*, 859.

Published on Web 03/12/2010

Besides, recent studies dealt with the solid solubility and phase transitions in the system $LaNb_{1-x}Ta_xO_4$,[17] and crystal chemistry of orthotantalates (La−Nd and Sm−Lu).[18] These works attempted for the difficulty to synthesize single-phase materials, particularly the tantalate ceramics, as well as the changes in the crystal structure along the lanthanide series. In this respect, many difficulties to determine the crystal chemistry of orthoceramics were successfully accomplished by using Raman spectroscopy under pressure.[16,19] In particular, it was shown that the structural sequences and transition pressures in orthocompounds are related with the packing efficiency of the anionic NbO_4 units around the RE cations.

To the best of our knowledge, there are no reports on the synthesis and vibrational spectroscopic studies of crystal structures for the complete series of lanthanide-orthoniobate ceramics. Particularly, polarized Raman scattering is not usual in studies of ceramic materials because of the intrinsic difficulties to discern and assign the active modes of unoriented samples, in contrast to oriented single-crystals. In view of the increasing importance of lanthanide orthoniobates for the materials chemistry and the lack of a comprehensive, widespread research of the complete RE series, we have decided to synthesize and investigate systematically the phonon modes of $RENbO_4$ ceramics (La−Lu, excluding radioactive promethium) through Raman and infrared spectroscopies. The results allow us to offer a synthesis route for these materials (there are no reports on the synthesis of $TmNbO_4$ material) and to determine the whole set of optical phonon modes for $RENbO_4$ compounds, in perfect agreement with group theory calculations, not yet reported in the literature. Finally, polarized Raman scattering was employed for the first time to investigate unoriented large- and small-grained $RENbO_4$ ceramics, which allowed us to establish the phonon symmetries of the Raman modes. It is straightforward to extend this method to any orthoniobate or orthotantalate material.

Experimental Section

$RENbO_4$ materials were synthesized by using RE_2O_3 (RE = La, Nd, Sm, Eu, Gd, Dy, Ho, Er, Tm, Yb, Lu; >99% Sigma-Aldrich), Tb_4O_7 (>99.9% Sigma-Aldrich), Pr_6O_{11} (>99.9% Sigma-Aldrich), CeO_2 (>99.9% Sigma-Aldrich), and Nb_2O_5 (>99.9% Sigma-Aldrich) as starting materials. Stoichiometric amounts of powder mixtures were mixed in alcohol or acetone and ground well. The mixed powders were calcined in the range 850−1250 °C for several hours, with intermediate regrinding. Sintered ceramics were produced by adding, when necessary, 1 wt % of polyvinyl alcohol (molecular weight ≈ 22 000, Sigma-Aldrich) and again dried and ground well. Cylindrical pucks of about 5 mm height and about 12.5 mm diameter were made by applying a pressure of 150 MPa. These compacts were then fired under microwaves (Milestone) at 1000 °C for 60 min to expel the binder, before being sintered in conventional oven at 1250 °C for times ranging from 4 to 9 h. The crystal structure and phase purity of the as-synthesized samples were studied by X-ray diffraction (XRD) using a Shimadzu D-6000 diffractometer with graphite monochromator and a nickel filter in the 2θ range 5−90°2θ (15 s/step of 0.02° 2θ), operating with Fe$K\alpha$ radiation (λ = 0.19360 nm), 40 kV, and 20 mA (the results were automatically converted to Cu$K\alpha$ radiation for data treatment and manipulation).

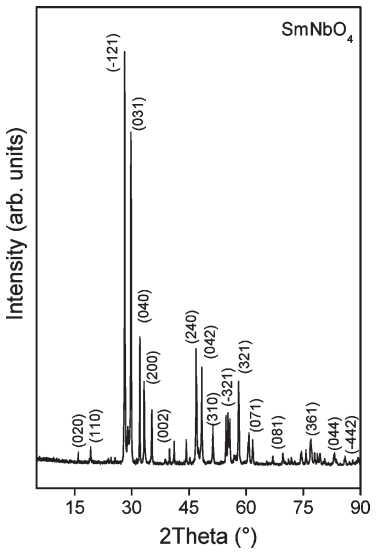

Figure 1. XRD pattern for the $SmNbO_4$ ceramics with the respective crystallographic planes, indexed by ICDD card 73−6080.

Raman spectra of as-synthesized samples were collected in backscattering configuration by using two different equipments. The first one was a triple-monochromator Jobin-Yvon T64000 spectrometer with an Olympus confocal microscope (80× objective), exciting lines of 488 and 514.5 nm of an Ar^+ laser (effective powers from 10 to 50 mW at the sample's surface), and a liquid-N_2-cooled charge coupled device (CCD) detector. The frequency resolution was better than 2 cm^{-1} and the accumulation times were typically 10 collections of 30 s. Also, an Horiba/Jobin-Yvon LABRAM-HR spectrometer was used with the 632.8 nm line of a helium−neon laser (effective power of 6 mW at the sample's surface) as excitation source, diffraction gratings of 600 and 1800 grooves/mm, Peltier-cooled CCD detector, confocal Olympus microscope (100× objective), and experimental resolution of typically 1 cm^{-1} for 10 accumulations of 30 s. All resulting spectra were corrected by the Bose−Einstein thermal factor.[20] Polarized Raman spectra were carried out in samples sintered at 1200 °C, for 8 hs. Appropriate interference filter for rejecting laser plasma lines, edge filter for stray light rejection, polarizers, and half-wave plate were used.

Fourier-transform infrared (FTIR) spectra in the mid-infrared region (500−4000 cm^{-1}) were collected in a Bomem equipment, model DA8−02, with a SiC source along with a Ge-coated KBr beamsplitter and a liquid nitrogen-cooled HgCdTe detector. In the far-infrared range (50−600 cm^{-1}), the SiC source, a 6 μm coated Mylar hypersplitter, and a liquid helium-cooled Si-bolometer were used. All measurements were conducted under vacuum (1×10^{-4} bar) in samples prepared as pressed-disks (150 MPa) by using a SpectraTech fixed-angle specular

(16) Hara, K.; Sawada, A.; Ishibashi, Y. *J. Phys. Soc. Jpn.* **1987**, *56*, 2187.
(17) Vullum, F.; Nitsche, F.; Selbach, S. M.; Grande, T. *J. Solid State Chem.* **2008**, *181*, 2580.
(18) Hartenbach, I.; Lissner, F.; Nikelski, T.; Meier, S. F.; Müller-Bunz, H.; Scheid, T. *Z. Anorg. Allg. Chem.* **2005**, *631*, 2377.
(19) Errandonea, D.; Manjón, F. J. *Prog. Mater. Sci.* **2008**, *53*, 711.
(20) Hayes W.; Loudon, R. *Scattering of Light by Crystals*; Wiley: New York, 1978.

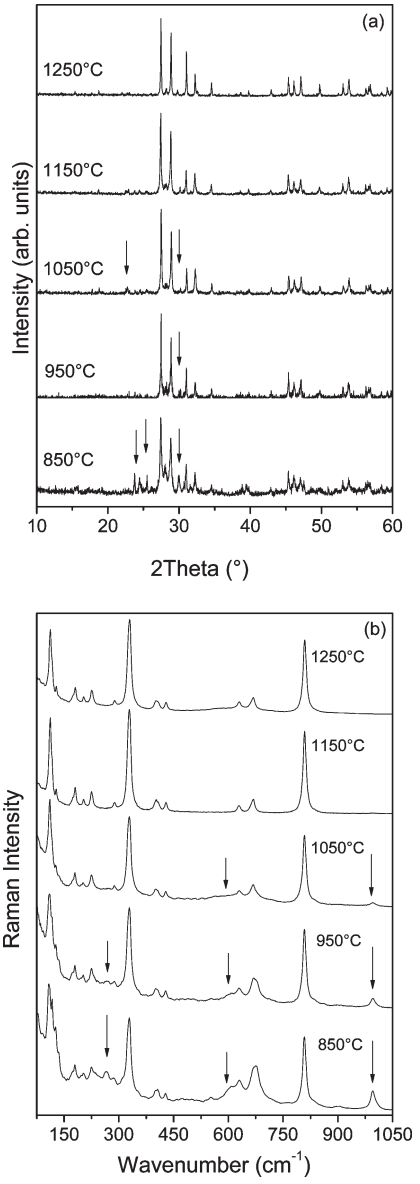

Figure 2. Thermal evolution for the $LaNbO_4$ compound in the temperature range 850−1250 °C probed by (a) XRD and (b) Raman scattering. Arrows indicate extra peaks and bands related to secondary phases, notably La_3NbO_7 and Nb_2O_5, which disappeared for higher heating temperatures.

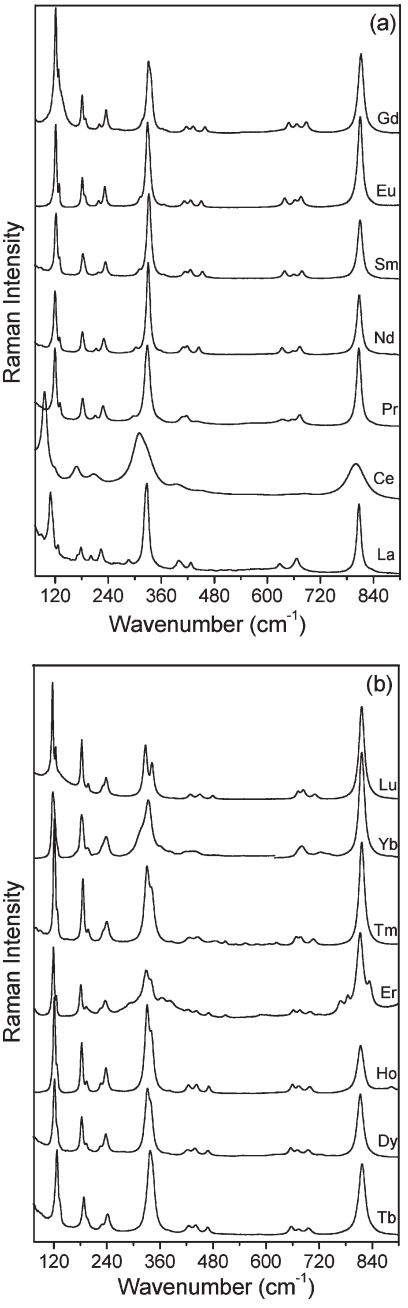

Figure 3. Raman spectra for all $RENbO_4$ materials obtained by solid-state reaction. The sequence plotted reproduces the variation (decreasing tendency) in the ionic radius: (a) La−Gd; (b) Tb−Lu.

reflectance accessory (external incidence angle of 11.5° and resolution of 4 cm^{-1}). The reflectivity spectra were evaluated by means of fitting procedures as well as by standard Kramers−Krönig calculations.

Results

Figure 1 presents a typical XRD pattern for the $SmNbO_4$ compound, which could be indexed with the ICDD (International Committee for Diffraction Data) card 73−6080. As can be seen, crystalline, single-phase ceramics were obtained after synthesis. All other samples exhibited similar patterns, only shifting to higher angles (lower *d*-spacings) along the lanthanide series from La to Lu, as expected. These two elements present opposed ionic radii in this series (coordination number is equal to 6):[21] La shows the higher value (1.032 Å), whereas Lu has the lower ionic radius (0.861 Å). The thermal evolution was probed by XRD and Raman scattering in order to set the optimum synthesis temperature. Figure 2 presents the XRD patterns (Figure 2a) besides the Raman spectra (Figure 2b) for $LaNbO_4$, as a function of the heating temperature. As it can be seen, the formation of the $LaNbO_4$ phase starts at 850 °C (the synthesis time was maintained constant in 2 hs for the experiments) with concurrent La_3NbO_7 and Nb_2O_5 oxides also present (see the arrows in Figure 2a). For temperatures of about 1150 °C, the $LaNbO_4$ phase stabilizes and residual reactants or secondary phases are no more observed. Raman

(21) Shannon, R. D. *Acta Crystallogr., Sect. A* **1976**, *32*, 751.

Table 1. Phonon Wavenumbers (cm^{-1}) and Assignment of the Gerade Modes, Determined from the Adjustment of the Raman Experimental Data by Lorentzian Lines for the Investigated $RENbO_4$ Ceramics

band	assignment	Lu	Yb	Tm	Er	Ho	Dy	Tb	Gd	Eu	Sm	Nd	Pr	Ce	La
1	A_g	117.1	117.6	122.5	118.9	121.1	121.6	127.3	121.6	121.6	122	119.8	119.4	95.8	109.6
2	A_g	118.5	122.0	124.7	121.6	124.2	124.2	130.4	123.8	124.2	125.1	122.9	122.5	103.0	115.4
3	B_g	124.7	127.8	128.2	126.0	127.3	127.8	134.4	128.2	129.1	129.6	130.0	130.9	120.2	126.9
4	A_g	183.2	183.2	185.9	181.5	183.2	183.2	188.1	181.0	181.5	182.8	181.9	182.3	156.6	169.9
5	B_g	197.9	196.5	198.3	193.0	194.3	193.4	197.4	189.0	187.7	187.0	185.9	185.4	168.1	178.8
6	B_g	230.7	227.6	230.2	226.7	226.3	224.9	228.0	220.0	218.3	218.3	212.1	210.7	199.6	201.0
7	B_g	238.2	238.2	240.0	236.5	237.8	237.8	241.8	235.1	232.5	233.8	229.8	228.5	207.2	224.0
8	B_g	315.8	304.3	307.9	311.9	310.5	318.5	308.8	316.7	312.7	310.1	303.0	297.2	268.7	286.6
9	A_g	327.4	316.3	330.5	327.8	331.4	332.3	338.0	331.4	329.2	331.8	330.9	328.7	310.5	327.4
10	B_g	342.5	334.5	341.1	339.8	340.7	337.6	343.3	337.1	336.3	335.8	335.0	334.9	328.3	332.3
11	B_g	390.4	362.4	386.8	424.1	382.4	379.7	381.0	362.4	366.4	367.0	358.9	357.1	347.3	346.5
12	B_g	429.0	385.0	425.8	442.7	424.5	422.3	425.0	417.0	412.1	413.4	409.4	406.3	390.4	392.6
13	B_g	450.2	418.3	445.4	471.1	442.3	439.2	441.4	432.5	426.7	426.3	418.8	417.4	396.6	399.7
14	A_g	480.0	444.5	487.1	508.3	470.2	468.9	468.0	459.1	450.7	452.9	444.5	443.6	454.7	427.2
15	B_g	672.9	681.3	668.5	661.8	660.0	656.0	656.9	648.5	639.2	639.2	633.0	634.3	653.8	628.1
16	A_g	684.4	723.5	677.8	676.9	674.2	671.1	674.2	667.1	662.3	660.5	657.4	656.5	677.3	658.3
17	B_g	710.6	741.7	707.1	699.1	698.6	695.5	696.4	688.0	676.5	678.2	673.3	673.3	687.1	667.1
18	A_g	816.6	816.2	816.6	812.6	814.0	813.1	817.1	812.2	810.0	810.0	807.7	807.3	801.1	807.3

spectra showed some extra bands related to Nb_2O_5[13] (indicated by arrows in Figure 2b) for temperatures up to 1050 °C, whereas pure $LaNbO_4$ Raman spectra can be visualized in temperatures above 1150 °C.

Raman spectra were obtained at room temperature for all the produced samples under optimized conditions of temperature and time. The results are displayed in Figure 3 (two boards) for decreasing ionic radius (La−Lu).[21] As can be noted, the samples exhibited very complex, similar spectra, as anticipated for identical crystal structures; the exceptions were $CeNbO_4$ and, in some aspects, $LaNbO_4$. For these samples, broader bands together with strongly down-shifted low-frequency modes were observed, which is probably linked to the proximity of a high temperature structural phase transition. Indeed, these compounds present a phase transition from monoclinic to tetragonal $I4_1/a$ structure, whose temperatures increase from La to Lu.[1,17] Also, some important differences should be noted. For example, the bands in the spectral range 316−343 cm^{-1} present a clear tendency to split for decreasing RE ionic radii, which probably result from lower degeneracy of modes for increasing monoclinic distortion. All samples were submitted to different Raman excitation lines because strong electronic transitions appeared for some conditions. The final spectra showed in Figure 3 represent the best results obtained using the blue line (488 nm), for Eu, Gd, Er, and Lu; green line (514.5 nm), for Ho and Yb; and the red line (632.8 nm), for La, Ce, Pr, Nd. Sm, Tb, Dy, and Tm.

At room temperature, $RENbO_4$ crystallizes in the monoclinic structure, space group $C2/c = C_{2h}^6$ (#15), with $Z = 4$. For this system, the cations RE and Nb occupy the 4e sites of C_2 symmetry, whereas the oxygen ions occupy the 8f sites with C_1 symmetry. Then, using the site group method of Rousseau et al.,[22] we can obtain the following distribution of the degrees of freedom at the Brillouin zone center in terms of the irreducible representations (i.r.) of the C_{2h} point group

$$\Gamma = 8A_g \oplus 10B_g \oplus 8A_u \oplus 10B_u \quad (1)$$

According to the character table of the C_{2h} point group, the acoustic modes are $A_u \oplus 2\ B_u$. Thus, we would expect 18 gerade Raman modes ($8\ A_g \oplus 10\ B_g$) and 15 ungerade IR bands ($7\ A_u \oplus 8\ B_u$) for this system. In view of the complexity of the spectra and the high number of compounds, a careful analysis was carried out by fitting the Raman experimental data with Lorentzian curves. The results evidenced all the eighteen bands, whose wavenumbers are summarized in Table 1. As an example, the spectrum of the $EuNbO_4$ ceramics is showed in Figure 4, which was divided up into three different wavenumber regions with numbered bands for better visualization. These results are in perfect agreement with the theoretical predictions.

Figure 5 presents the wavenumbers of the Raman-active bands as functions of ionic radii[21] for all materials studied here. We observe that all wavenumbers, except the bands numbered 1 and 3 at around 117 and 125 cm^{-1} (Figure 5a), decrease for increasing ionic radii, as expected. The phenomenon is well-known as lanthanide contraction (crystal radii of the RE ions decrease for increasing atomic number) and lead to a closer packing of the NbO_4^{-3} units from La to Lu, which reduces the Nb−O distances to yield higher frequencies for smaller RE ions. The low-wavenumber bands are frequently interpreted as external modes, considering that $RENbO_4$ could be visualized as two sublattices: RE ions plus NbO_4 units. For these bands, an inverse phenomenon was observed that can be attributable to a mass effect. Thus, these bands are related primarily to the RE ions, if one considers that the harmonic approximation is valid. Other bands displayed in panels a and b in Figure 5 (2, 4, 8, 9, and 10) remain practically unchanged for varying RE ions, which can be understood by considering a compensating balance between the lanthanide contraction (tends to increase the wavenumbers for decreasing ionic radii) and the mass effect for these particular modes

(22) Rousseau, D. L.; Bauman, R. P.; Porto, S. P. S. *J. Raman Spectrosc.* **1981**, *10*, 253.

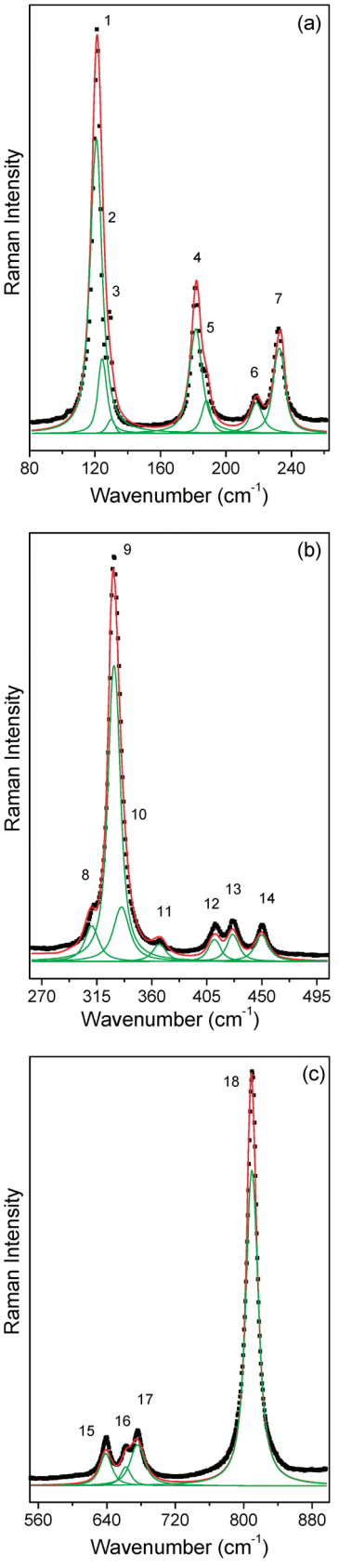

Figure 4. Micro-Raman spectrum for $EuNbO_4$ ceramics in the spectral region 80−900 cm^{-1}: (a) 80−260 cm^{-1}; (b) 260−500 cm^{-1}; and (c) 550−900 cm^{-1}. Experimental data are in closed squares, whereas the fitting curves are represented by red lines. Green lines represent the phonon modes adjusted by Lorentzian curves. The Raman-active modes were numbered for better visualization.

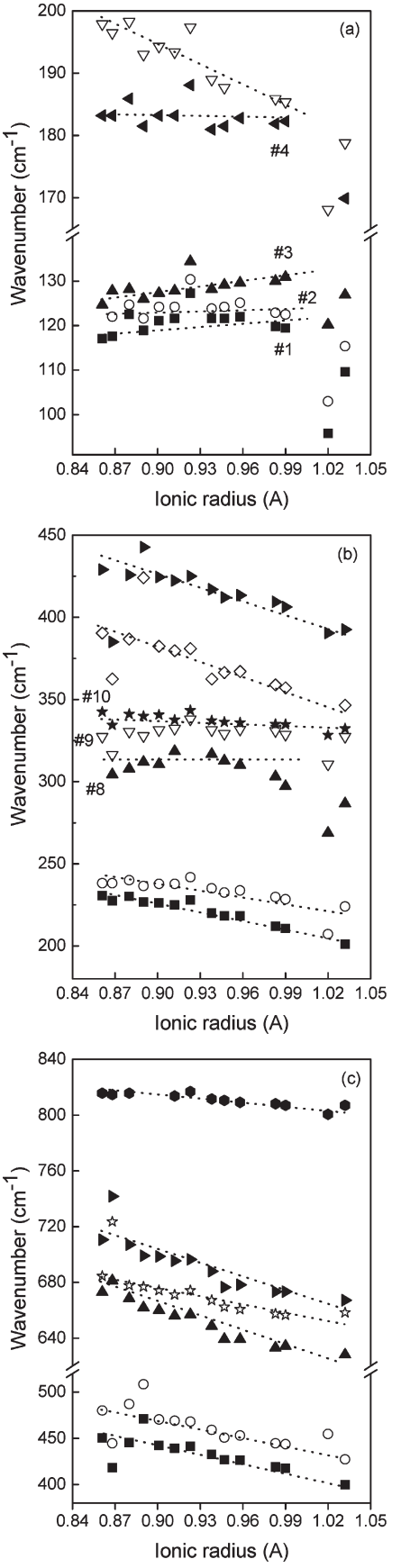

Figure 5. Phonon wavenumbers for the discerned Raman-active modes as a function of ionic radii for all the $RENbO_4$ materials. The dotted lines are guide for the eyes.

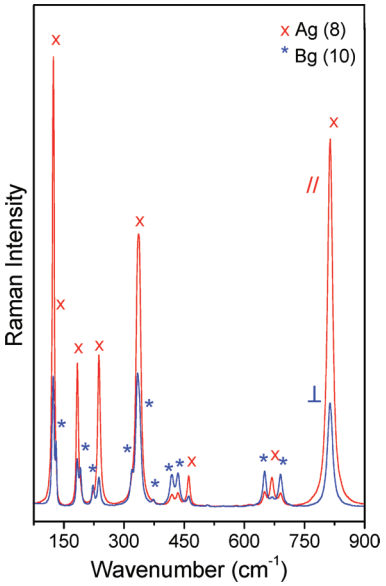

Figure 6. Polarized Raman scattering for the sintered $GdNbO_4$ ceramic. Parallel- (//) and cross-polarized (⊥) configurations are indicated in red and blue lines, respectively. The ten B_g modes isolated by the cross-polarized Raman scattering are indicated by blue asterisks, whereas the eight A_g bands were identified by red crosses.

(dominated by the mass of NbO_4 unit rather than the RE mass). This result was previously verified in RE orthovanadates[23] for B_{1g} translational-type modes related to out-of-phase and in-phase movements of the RE and VO_4 units. Finally, it is important to note the sudden downshift of the low-wavenumber modes, particularly those below 200 cm^{-1} for $LaNbO_4$ and $CeNbO_4$ materials (Figure 5a). For these compounds, this result must undoubtedly be associated to a soft mode behavior (even verified at room temperature) because of the lower phase-transition temperatures compared with the other analogues. The literature reports transition temperatures of about 480−520 °C for La,[1,17] whereas there are no reports on $CeNbO_4$ material. We believe that this temperature is even lower because of the broadness and the down-shifted frequencies verified for this compound. The study of phase transitions (monoclinic to tetragonal) in these materials is in due course and will be published elsewhere.

Now, the results of polarized Raman scattering will be presented. The inelastic light scattering intensities due to the Raman effect are proportional to the square of the elements of the polarizability tensor, a second-order tensor. The base functions of the i.r. that contain the Raman-active modes then have a quadratic form, i.e., they transform like the product of the Cartesian coordinates. When dealing with crystals, we take benefit of the crystal symmetry to assign the lattice vibrations to the different i.r.[20,22] However, in the case of ceramics, although the group-theory predictions remain valid, the symmetry of modes are generally mixed because of the random orientation of the small crystalline grains. In this work, we have used a confocal microscope with an objective of magnification of 100×, which allows the

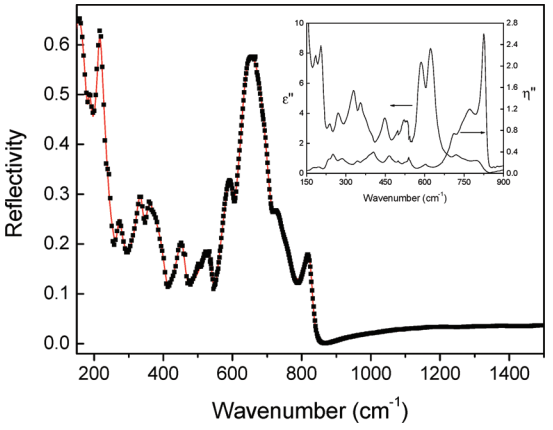

Figure 7. Measured (closed squares) and adjusted (solid red line) infrared reflectivity spectra for the $NdNbO_4$ sintered sample. Inset: Imaginary parts of the direct ($\varepsilon''(\omega)$, left curve) and reciprocal ($\eta''(\omega)$, right curve) dielectric functions, obtained from Kramers−Krönig analysis of the infrared reflectance data for the $NdNbO_4$ compound.

selection of an observation region as small as 2 μm on the sample surface or even inside the sample. All samples were sintered at 1200 °C, for 8 h, and then analyzed by polarized Raman spectroscopy. It is important to note that we do not know anything about the crystallographic axes inside the grains, which have also random orientation throughout the sample. By measuring the micro-Raman spectra of $RENbO_4$ sintered sample with cross-polarized light, we displaced the sample under the microscope looking for spectral changes. We observed that for some grains the spectra of parallel and crossed light became different, as exemplified in Figure 6 for $GdNbO_4$. For different grains, we always observed the relative strengthening of the bands around 128, 189, 220, 317, 337, 362, 417, 433, 649, and 688 cm^{-1} with cross-polarized light, accompanied by the relative weakening of bands at 122, 124, 181, 235, 331, 459, 667, and 812 cm^{-1}. Therefore, we could assign these Raman-active modes as belonging to the B_g and A_g symmetries, respectively. This result is introduced in Table 1 for all samples.

The infrared reflectivity spectrum of $NdNbO_4$ is presented in Figure 7. This spectrum has been analyzed by using the four-parameter semiquantum model,[24] using a nonlinear least-squares program.[25] According to this model, the infrared phonon contribution to the complex dielectric function $\varepsilon(\omega)$ is given by:

$$\varepsilon(\omega) = \varepsilon_\infty \prod_{j=1}^{N} \frac{\Omega_{j,\mathrm{LO}}^2 - \omega^2 + i\omega\gamma_{j,\mathrm{LO}}}{\Omega_{j,\mathrm{TO}}^2 - \omega^2 + i\omega\gamma_{j,\mathrm{TO}}} \qquad (2)$$

where ε_∞ is the dielectric constant due to the electronic polarization contribution, $\Omega_{j,\mathrm{LO}}$ ($\Omega_{j,\mathrm{TO}}$) and $\gamma_{j,\mathrm{LO}}$ ($\gamma_{j,\mathrm{TO}}$) are the frequency and damping of the jth longitudinal (transverse) optical modes, respectively. N is the number of polar phonons. At quasinormal incidence, the

(23) Santos, C. C.; Silva, E. N.; Ayala, A. P.; Guedes, I.; Pizani, P. S.; Loong, C.-K.; Boatner, L. A. *J. Appl. Phys.* **2007**, *101*, 053511.
(24) Gervais F.; Echegut, P. In *Incommensurate Phases in Dielectrics*; Blinc, R., Levanyuk, A. P., Eds.; North Holland: Amsterdam, 1986; p 337.
(25) Meneses, D. D.; Gruener, G.; Malki, M.; Echegut, P. *J. Non-Cryst. Solids* **2005**, *351*, 124.

Table 2. Phonon Dispersion Parameters of the Ungerade Modes Calculated from the Fit of the Infrared Reflectance Spectrum of $NdNbO_4$

phonons	$\Omega_{j,TO}$ (cm^{-1})	$\gamma_{j,TO}$ (cm^{-1})	$\Omega_{j,LO}$ (cm^{-1})	$\gamma_{j,LO}$ (cm^{-1})	$\Delta\varepsilon_j$
1	150.3	17	183.5	16	6.6839
2	185.3	11	192.9	8	0.1446
3	193.1	7	196.2	19	0.0080
4	200.1	19	211.6	29	0.2525
5	212.0	13	247.3	93	0.0198
6	270.9	15	271.4	23	0.0055
7	333.7	28	343.2	19	0.2266
8	350.4	28	356.5	86	0.0498
9	405.5	54	408.2	33	0.0446
10	453.0	29	462.3	29	0.1500
11	540.2	33	544.7	18	0.0963
12	589.0	26	599.7	28	0.2904
13	627.9	34	713.7	39	0.5834
14	721.3	35	748.2	101	0.0144
15	820.5	45	829.9	17	0.0216
	ε_∞ = 2.51	ε_r = 11.10			

dielectric function is related to the optical reflectivity R by the Fresnel formula

$$R = \left|\frac{\sqrt{\varepsilon(\omega)}-1}{\sqrt{\varepsilon(\omega)}+1}\right|^2 \quad (3)$$

Equations 2 and 3 were used to fit the experimental data and the results are also presented in Figure 7 as a solid red curve. We could then obtain the wavenumbers and widths of the transverse (TO) and longitudinal (LO) infrared branches, which are listed in Table 2. We note that 15 infrared modes were discerned for this material after fitting. To corroborate the results obtained with the fitting procedures, the imaginary parts of ε (dielectric function) and of $1/\varepsilon = \eta$ were calculated independently by using Kramers-Krönig analysis[20] and are presented as inset in Figure 7. These optical functions were studied because they give, respectively, the values of the TO (transverse optical) and LO (longitudinal optical) mode frequencies. These values can be compared with those obtained from fitting of the raw data in Figure 7, with the advantage of studying individual phonon contributions without any physical inconsistency. Indeed, there is a very good agreement between the phonon modes observed by Kramers−Krönig (Figure 7) and those calculated through fitting with the four-parameter oscillator model (Table 2).

Once the infrared modes were determined, the oscillator strengths of the individual jth TO modes can be obtained by

$$\Delta\varepsilon_j = \frac{\varepsilon_\infty}{\Omega_{j,TO}^2} \times \frac{\prod_k(\Omega_{k,LO}^2 - \Omega_{j,TO}^2)}{\prod_{k\neq j}(\Omega_{k,TO}^2 - \Omega_{j,TO}^2)} \quad (4)$$

The static (infrared) dielectric constant, which corresponds to the intrinsic microwave dielectric constant, can then be obtained by adding the oscillator strengths over all modes, i.e.

$$\varepsilon_r = \varepsilon_\infty + \sum_{j=1}^{N} \Delta\varepsilon_j \quad (5)$$

The values of ε_j, ε_r, and ε_∞ for $NdNbO_4$ are given in Table 2, together with the phonon modes parameters. Although the measurements were carried out in high density, sintered ceramics, a low value for the ε_r was observed ($\varepsilon_r = 11.1$), if compared with the value reported by Kim et al.[1] ($\varepsilon_r = 19.6$). This result is probably related to the presence of extrinsic defects in the prepared sample, which decrease substantially ε_r.

Conclusions

Lanthanide orthoniobate materials (La, Ce, Pr, Nd, Sm, Eu, Gd, Tb, Dy, Ho, Er, Tm, Yb, Lu) were synthesized by solid-state reactions and their crystal structures were systematically investigated by vibrational spectroscopy. Crystalline, single-phase materials were produced at optimized synthesis conditions of temperature and time. XRD, Raman scattering and infrared spectroscopy were employed to investigate the crystal structures of this lanthanide orthoniobate series. All $RENbO_4$ ceramics exhibit a monoclinic $C2/c$ (No. 15) structure, with $Z = 4$. Raman spectroscopy showed 18 active-modes that could be discerned and assigned through polarized Raman scattering, in perfect agreement with group-theory calculations. The majority of bands presented a decreasing tendency of the phonon wavenumbers for increasing ionic radii, which is a consequence of the lanthanide-induced unit-cell expansion. Bands that increase their wavenumbers for increasing ionic radius are rather influenced by a mass effect. Fourier-transform infrared spectroscopy was employed to study the optical polar phonons of these materials. The results showed fifteen active-modes after fitting, as predicted by the group-theory. Kramers−Krönig analysis was used to corroborate these results and to establish a complete set of active phonons, not yet reported in the literature.

Acknowledgment. The authors acknowledge financial support from CNPq, FINEP, and FAPEMIG. Special thanks to Prof. M. A. Pimenta (UFMG) for his hospitality during Raman experiments with the Jobin-Yvon T64000 equipment.